Powder Technology 339 (xxxx) 633–640

Contents lists available at ScienceDirect

Powder Technology

journal homepage: www.elsevier.com/locate/powtec

Investigation into the elutriation of fines from binary mixtures via CFD simulation with a multi-scale drag model

Shuai Wang *, Bang Hu, Siyu Liu, Weijie Yin, Kai Zhang

School of Energy Science and Engineering, Harbin Institute of Technology, Harbin 150001, China

ARTICLE INFO

Article history:
Received 14 April 2018
Received in revised form 13 August 2018
Accepted 15 August 2018
Available online 23 August 2018

Keywords:
Elutriation
Fluidized bed
Drag
Multi-fluid model
Bubble

ABSTRACT

In the coal-direct chemical looping combustion process, the separation of char and ash from oxygen carriers is essential for reducing the requirement of fresh oxygen carriers and avoiding the char into the air reactor. In this work, a three-dimensional simulation is conducted to investigate the solid-solid separation process in a fluidized bed reactor by means of the multi-fluid model, where the multi-scale drag model is implemented to describe the bubble effect in the bed. The elutriation process of fine particles from mixture is evaluated. The model prediction is compared with the experimental results. The results demonstrate that the dependence of the elutriation rate on fine particle diameter is not monotonous owing to the formation of agglomeration. Meanwhile, the increase of operating temperature promotes the non-uniform degree of interphase drag force and the elutriation rate of fine particles is reduced.

1. Introduction

Chemical looping combustion (CLC), as a promising combustion technology with inherent CO_2 separation, has drawn more and more concerns [1–3]. Solid fuels have been successfully applied in the CLC process owing to their wide availability and low cost [4–7]. Wadhwani et al. [8] evaluated the ash effect on the CLC with coal as fuel using computational fluid dynamics (CFD) approach. It was demonstrated that the coal with different ash fractions influenced the overall fuel conversion. In order to avoid char and ash entering the air reactor to achieve the carbon capture and prevent the ash accumulation in the surface of oxygen carriers, ash and char separation from oxygen carriers appears very important. Employing the particles with different aerodynamic characteristics provides a possibility for the solid-solid separation. Hence, it is necessary to analyze the solid holdup in the bed and the elutriation rate of fine particles from the bed to get a better optimization of solid-solid separation process in the system.

Monazam et al. [9] experimentally studied the elutriation of fine particles in a bubbling fluidized bed with binary mixture. By evaluating the influence of physical properties and operating parameters, it was found that the elutriation rate of fines was more sensitive to the initial loading of fines and operating velocity. Choi et al. [10] investigated the impact of fine particles on the elutriation rate of coarse particles in a fluidized bed by means of experimental methods. The results revealed that the effect of fine particles on elutriation of coarse particles was weakened with the increase of gas velocity. The bed particle size distribution had no influence on the elutriation of fine particles. Azadi et al. [11] employed the multi-fluid model to investigate the performance of limestone particles' elutriation in a fluidized bed. It was pointed out that a small particle size resulted in a high elutriation rate. The effect of cohesive force was less significant for larger particle size. Although some studies have been done on the particles' elutriation in a fluidized bed, there are few reports on the particles' elutriation under the high temperature condition.

In the simulation of fluidized beds, the interphase drag force plays an important role in the accuracy of model prediction. Schneiderbauer et al. [12] conducted a comparative analysis of subgrid drag modifications for a bubbling fluidized bed and emphasized that the homogenous drag law could not give a good prediction on a bubbling fluidized bed with coarse grids. It is necessary to combine the subgrid drag modifications to reflect the effect of unresolved structures. In order to describe the effect of non-uniform structures caused by clusters and bubbles in a fluidized bed, the energy minimization multi-scale (EMMS) model was proposed, which has been successfully applied in the gas-solid flow in a fluidized bed [13–15]. Most of the EMMS drag models have been developed for the mono-component particle flow, which are restrictive in the multi-component particles system. Lungu et al. [16] extended the bubble-based EMMS model to the bi-disperse system. The model prediction gave a better agreement with experimental values compared to that using the traditional drag model. Zhou et al. [17] developed the EMMS drag model for the binary gas-solid flow and investigated the mixing and segregation behaviors in a CFB riser. It was pointed out that the proposed drag model with the kinetic theory of binary mixture could reasonably predict the mixing and segregation patterns in risers.

* Corresponding author.
E-mail address: shuaiwang@hit.edu.cn (S. Wang).

https://doi.org/10.1016/j.powtec.2018.08.047
0032-5910/

In this work, the elutriation of fine particles in a fluidized bed with binary mixture is investigated using the multi-fluid model, where the kinetic theory of binary mixture is employed and a bubble-based multi-scale drag model of bi-dispersed particles is implemented to account for the effect of mesoscale structures in a fluidized bed. The dependence of the elutriation rate on operating conditions and physical parameters is analyzed. The model prediction can give a fair agreement with experimental results. The impact of operating temperature on the multi-scale drag coefficient is examined. The elutriation process of fine particles at a high temperature is evaluated.

2. Numerical method

2.1. Multi-fluid model

In the current work, the multi-fluid model is used to describe the separation behaviors of binary mixture and elutriation of fine particles in a fluidized bed. It is assumed that the solid phases are spherical with their respective uniform size. Granular temperature is introduced to measure the variation of fluctuating energy of particles. The main governing equations comprise mass and momentum conservation equations of gas and solid phases as well as granular temperature transportation equation. The kinetic theory of a polydisperse system is adopted to close the model [18]. In order to characterize the frictional contribution between particles at a high solid volume fraction below maximum packing, a modification of Savage friction stress model proposed by Srivastava et al. [19] is adopted, where the strain-rate fluctuations are further taken into consideration. The detailed governing equations and closure models are summarized in Table 1 [20].

2.2. Bubble-based drag model of binary mixture

Bubbles are regarded as mesoscale structures in a bubbling fluidized bed. The bed non-uniformity caused by bubbles influences the gas-solid interaction, which makes the model prediction more complicated in a binary mixture system. Shi et al. [14] proposed a bubble-based EMMS model for a mono-disperse system to account for the bubble effect, which was further extended to a bi-disperse system considering the difference of physical properties of particles [20]. The different particle phases have their respective volume fractions (ε_{es1}, ε_{es2}) and superficial velocities (U_{pe1}, U_{pe2}). It is assumed that the particle only exists in the emulsion phase. The mean properties of the emulsion phase are written as below [21]:

$$\rho_e = \rho_{p1}\varepsilon_{es1} + \rho_{p2}\varepsilon_{es2} + \rho_g\varepsilon_e \tag{1}$$

$$\mu_e = \mu_g\left[1 + 2.5(1-\varepsilon_e) + 10.05(1-\varepsilon_e)^2 + 0.00273\ \exp(16.6(1-\varepsilon_e))\right] \tag{2}$$

$$U_e = \frac{\rho_g U_{ge} + \rho_{p1}U_{pe1} + \rho_{p2}U_{pe2}}{\rho_e} \tag{3}$$

The bubble-based drag force includes the inter-phase force in the emulsion phase and the bubble-induced contribution. The drag coefficients of bi-disperse particles are expressed as follows:

$$\beta_1 = \frac{\varepsilon_g^2}{U_{slip}}\left[\frac{3}{4}C_{de1}\frac{(1-\delta_b)\varepsilon_{es1}}{d_{p1}}\rho_g {U_{se1}}^2 + \delta_b\left(\rho_{p1}-\rho_g\right)\varepsilon_{es1}(g+a_b)\right] \tag{4}$$

$$\beta_2 = \frac{\varepsilon_g^2}{U_{slip}}\left[\frac{3}{4}C_{de2}\frac{(1-\delta_b)\varepsilon_{es2}}{d_{p2}}\rho_g {U_{se2}}^2 + \delta_b\left(\rho_{p2}-\rho_g\right)\varepsilon_{es2}(g+a_b)\right] \tag{5}$$

From the above equations, we have to obtain the local structural parameters for the solution of drag coefficient, which requires the establishment of the corresponding equations or relations. The detailed expressions are summarized in Table 2 [20]. A stability criterion of the minimum suspending energy consumption is introduced to achieve the model closure. For the simulation of the CLC process under high temperature operation, the bed non-uniformity and the multi-scale interphase drag is influenced by a significant variation of physical properties, which will be further discussed in the next section.

Table 1
Governing equations and closure models in this work [20].

1. Continuity equations	(T1–1)
$\frac{\partial}{\partial t}(\varepsilon_g\rho_g) + \frac{\partial}{\partial x_i}(\varepsilon_g\rho_g u_g) = 0$	
$\frac{\partial}{\partial t}(\varepsilon_m\rho_m) + \frac{\partial}{\partial x_i}(\varepsilon_m\rho_m u_{mi}) = 0$	(T1–2)
2. Momentum conservation equations	(T1–3)
$[\frac{\partial}{\partial t}(\varepsilon_g\rho_g u_{gi}) + \frac{\partial}{\partial x_j}(\varepsilon_g\rho_g u_{gj}u_{gi})] = -\varepsilon_g\frac{\partial P_g}{\partial x_j} + \frac{\partial \tau_{gji}}{\partial x_j} + \varepsilon_g\rho_g g_i\text{-}\beta_{gm}(u_{gi}-u_{mi})$	
$[\frac{\partial}{\partial t}(\varepsilon_m\rho_m u_{mi}) + \frac{\partial}{\partial x_j}(\varepsilon_m\rho_m u_{mj}u_{mi})] = -\varepsilon_m\frac{\partial P_g}{\partial x_j} + \frac{\partial \tau_{mij}}{\partial x_j} + \varepsilon_m\rho_m g_i + \beta_{gm}(u_{gi}-u_{mi}) + \sum_{l\neq m}\beta_{lm}(u_{li}-u_{mi})$	(T1–4)
3. Granular temperature transportation equations for solid phases	(T1–5)
$\frac{3}{2}\varepsilon_m\rho_m[\frac{\partial\Theta_m}{\partial t} + u_{mj}\frac{\partial\Theta_m}{\partial x_j}] = \frac{\partial}{\partial x_j}(\kappa_m\frac{\partial\Theta_m}{\partial x_j}) + \tau_{mij}\frac{\partial u_{mi}}{\partial x_j} + \prod_m - J_m$	
4. Solid stress tensor	(T1–6)
$\tau_{mij} = (-P_m + \eta\mu_b\frac{\partial u_{mi}}{\partial x_i})\delta_{ij} + \mu_m([\frac{\partial u_{mi}}{\partial x_j} + \frac{\partial u_{mj}}{\partial x_i}] - \frac{2}{3}\frac{\partial u_{mi}}{\partial x_i})$	
$\mu_m = (\frac{2+\alpha}{3})[\frac{\mu_m^*}{g_{0,mn}\eta(2-\eta)}(1 + \frac{8}{5}\eta\sum_{n=1}^{M}(\varepsilon_n g_{0,mn}))(1 + \frac{8}{5}\eta(3\eta\text{-}2)\sum_{n=1}^{M}(\varepsilon_n g_{0,mn})) + \frac{3}{5}\eta\mu_b]$	(T1–7)
$\mu_m^* = \frac{\varepsilon_m\rho_m g_{0,mn}\Theta_m\mu}{\rho_m\sum_{n=1}^{M}(\varepsilon_n g_{0,mn})\Theta_m + (\frac{2\eta_{ij}}{\rho_m\varepsilon_m})}\mu = \frac{5}{96}\rho_m d_p\sqrt{\pi\Theta_m}$	(T1–8)
$\mu_b = \frac{256}{5\pi}\mu\varepsilon_m\sum_{n=1}^{M}(\varepsilon_n g_{0,mn})\eta = \frac{1+e}{2}$	(T1–9)
5. Solid pressure	(T1–10)
$P_m = \varepsilon_m\rho_m\Theta_m[1 + 4\eta\sum_{n=1}^{M}(\varepsilon_n g_{0,mn})]$	
6. Thermal conductivity of particles	(T1–11)
$\kappa_m = (\frac{\kappa_m^*}{g_{0,mn}})[(1 + \frac{12}{5}\eta(\varepsilon_n g_{0,mn}))(1 + \frac{12}{5}\eta^2(4\eta-3))\sum_{n=1}^{M}(\varepsilon_n g_{0,mn}) + \frac{64}{25\pi}(41-33\eta)\eta^2(\sum_{n=1}^{M}(\varepsilon_n g_{0,mn}))^2]$	
7. Collisional dissipation	(T1–12)
$J_m = \frac{48}{\sqrt{\pi}}\eta(1-\eta)\frac{\sum_{n=1}^{M}(\varepsilon_n g_{0,mn})}{d_p}\Theta_m^{3/2}$	
8. Kinetic energy production through slip between phase	(T1–13)
$\Pi_m = -3\beta\Theta_s + \frac{81\varepsilon_m\mu_g^2\lvert u_g-u_m\rvert^2}{g_{0,mn}d_p^2\rho_m\sqrt{\pi\Theta_m}}$	

Table 2
Balance equations and relations in the bubble-based drag model [20].

1. Force balance equations in the emulsion phase	(T2–1)
$\frac{3}{4}C_{de1}\frac{\varepsilon_{es1}}{d_{p1}}\rho_g {U_{se1}}^2+\frac{3}{4}C_{de2}\frac{\varepsilon_{es2}}{d_{p2}}\rho_g {U_{se2}}^2=(\rho_{p2}-\rho_g)\varepsilon_{es2}(g+a_e)+(\rho_{p1}-\rho_g)\varepsilon_{es1}(g+a_e)$	
2. Force balance equations for bubble phase	(T2–2)
$\frac{3}{4}C_{db}\frac{1}{d_b}\rho_e {U_{sb}}^2=(\rho_e-\rho_g)(g+a_b)$	
3. Mass conversion of gas and particles in the grid	(T2–3)
$U_g=U_{ge}(1-\delta_b)+\delta_b U_b U_{p1}=U_{pe1}(1-\delta_b)\ U_{p2}=U_{pe2}(1-\delta_b)$	
4. Definition of overall gas and solid volume fraction	(T2–4)
$\varepsilon_g=(1-\delta_b)\varepsilon_e+\delta_b\varepsilon_s=(1-\delta_b)(\varepsilon_{es1}+\varepsilon_{es2})$	
5. stability criterion of the minimum suspending energy consumption	(T2–5)
$N_s=\frac{1}{(\rho_e-\rho_g)}(\frac{3}{4}C_{de1}\frac{\varepsilon_{es1}}{d_{p1}}\rho_g {U_{se1}}^2+\frac{3}{4}C_{de2}\frac{\varepsilon_{es2}}{d_{p2}}\rho_g {U_{se2}}^2)U_{ge}+f_b U_g(g+a_b)\rightarrow$ min	

2.3. Elutriation rate description

With regard to the description of the elutriation from a fluidized bed, some models have been developed [22,23]. The model proposed by Kato et al. [24] is adopted and expressed as follows:

$$W_e = W_{f0}\left(1-e^{-kt}\right) \tag{6}$$

Where W_e and W_{f0} represent the cumulative mass of fines out of the bed and initial total mass in the bed. k denotes the elutriation rate constant.

2.4. Simulation implementation and system description

On the basis of the experimental apparatus of Monazam et al. [9], a three-dimensional simulation is carried out to investigate the elutriation process of fines from binary mixture in a fluidized bed, which has a height of 1.7 m and a diameter of 0.1 m, as shown in Fig. 1. The glass beads and Ilmenite are chosen as the fine and coarse particles, which have mean diameters of 0.093 mm and 0.309 mm, and averaged densities of 2464 kg/m^3 and 3968 kg/m^3 respectively. The particles are initially loaded at the bottom of the bed with the static bed height of 0.0762 m. The air distributor locates between the bed and the air plenum. The fluidizing air inlet is set at the side of the air plenum with a specified velocity. The pressure outlet is specified at the top of the bed with an atmospheric pressure. For the wall, the no-slip boundary condition is applied to gas phase and the solid phases adopt the partial slip boundary condition [25]. The detailed parameters and operating conditions are listed in Table 3 [9].

The model is implemented on the platform of the MFIX program, which is a professional open-source CFD code for the simulation of the multiphase flow [26]. The bubble-based drag model is programmed and incorporated into the multi-fluid model. The higher order Total Variation Diminishing (TVD) scheme is employed as the discretization scheme, which incorporates a modification into the higher order upwind scheme for hyperbolic systems. In order to increase the computational efficiency, the auto-adjustable time step of 1×10^{-6}–1×10^{-4} s is adopted. A mesh-independence investigation is performed using different grids. Considering the accuracy and computing cost, the mesh size of 6 mm × 10 mm × 6 mm is chosen as the final computational grid size. The total simulation time lasts for 30s, costing about 3–4 days on a PC with 2.7 GHz CPU and 16 GB RAM.

3. Results and discussion

In order to validate the model, the simulated cumulative mass of fines out of the bed with time is compared with experimental results, as show in Fig. 2. It can be observed that the prediction using the bubble-based drag model can give a good agreement with measured data. The discrepancy between the model prediction and experimental values may be attributed to the uncertainty of air distributor resistance. Meanwhile, the delay error of collecting fines may be also a reason. The simulated result using the traditional Gidaspow drag model is also displayed in Fig. 2. More fines mass out of the bed is predicted with the Gidaspow drag model, which has an overestimation on the measured value. This is because the traditional drag model over-predicts the gas driving force, leading to a higher bed expansion and the enhancement of the elutriation process of fines. Hence, the consideration of the bubble effect is necessary in the simulation.

The heterogeneous index is introduced to reflect the effect of the bubble-based multiscale drag and the variations with voidage for binary particles are displayed in Fig. 3. We can observe that the increase of fine particle fractions reduces the heterogeneous index, which means the non-uniformity of the bed is enhanced. Moreover, the influencing

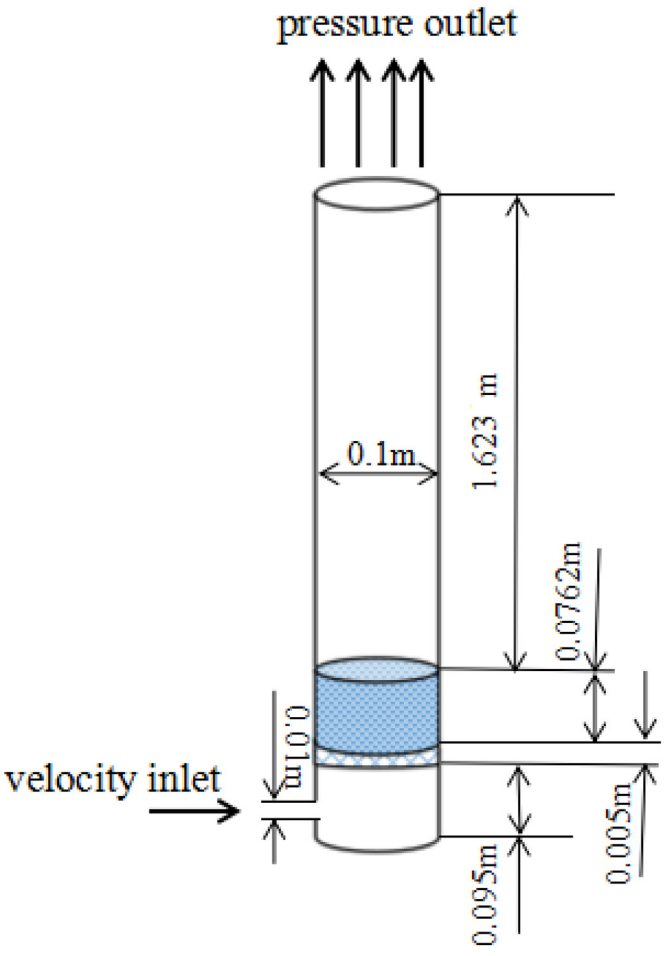

Fig. 1. Schematic diagram for a bubbling fluidized bed.

Table 3
Main operating parameters in the simulation [9].

Description	Simulation	Unit
Reactor height	1.7	m
Reactor diameter	0.1	m
Particle density	2464/3968	kg/m^3
Mean particle diameter	$9.3 \times 10^{-5}/3.09 \times 10^{-4}$	m
Initial solid height	0.0762	m
Initial particle volume fraction	0.41/0.19	–
Initial temperature	298	K
Inlet gas velocity	0.39,0.47,0.59,0.78	m s^{-1}
Pressure outlet	1.013×10^5	Pa

range of fine particles is wider, which implies that fine particles tend to form the mesoscale structures. Hence, we can realize that the drag coefficient in a bi-disperse system does not only depend on the voidage but on its own solid component fraction.

Fig. 4 shows the contour plots of solid concentrations under different operating velocities. It can be clearly recognized that more fine particles are elutriated at a high velocity. Although the bed height of large particles is improved with the increase of operating velocity, the effect is less significant. In addition, we can distinguish that a high operating velocity can enhance the particle fluctuating degree in the bed and the formation of meso-scale structures is more obvious.

Fig. 5 demonstrates the lateral profiles of axial solid velocity at different operating velocities. We can find that the solid velocity is positive with an unclear variation in the center zone and decreases towards the wall. The negative value of solid velocity near the wall means the down-flow of particles owing to the wall friction. The increase of operating velocity enhances the lateral difference of solid velocity between the center and the wall. In contrast, the upflow of fine particles is more significant and the velocity of coarse particles near the wall is greater, which reflects the segregation behaviors of binary mixture and the elutriation process of fine particles in some degree.

Fig. 6 illustrates the lateral profiles of granular temperature of binary mixture at different operating velocities. It can be clearly observed that the increase of operating velocity promotes the granular temperature. This is attributed to the fact that the solid volume fraction is reduced at a high operating velocity so that the mean free path of particles is enlarged, resulting in the increase of the solid fluctuating energy. In contrast, coarse particles have greater granular temperatures than fine particles, which is related to the solid component fraction distribution.

From the Eq. (6), the cumulative mass of fine particles with time shows an exponential growth. The variation of $\ln(1 - W_e/W_{f0})$ with time is plotted in Fig. 7. It can be clearly found that there is almost a linear dependence between $\ln(1 - W_e/W_{f0})$ and time t. The slope of the straight line refers to the elutriation rate constant. We can see that the increase of operating velocity promotes the elutriation rate constant, which is consistent with the experimental results obtained by Monazam et al. [9]. In order to better characterize the elutriation rate of fines leaving the bed, the normalized elutriation rate constant K^* is written in the following expression [6]:

$$K^* = \frac{kW_{f0}}{A_b} \tag{7}$$

The dependence of the normalized elutriation rate constant on operating velocity and initial loading of fines is investigated and shown in Fig. 8. We can realize that the variations of the normalized elutriation rate constant with operating velocity and initial loading of fines show an exponential growth in different extents. Compared to the effect of operating velocity, the elutriation rate constant is more sensitive to the initial loading of fines. The measured values by Monazam et al. [9] are also shown in Fig. 8. It can be seen that the model prediction can give a fair agreement with the experimented result, which implies

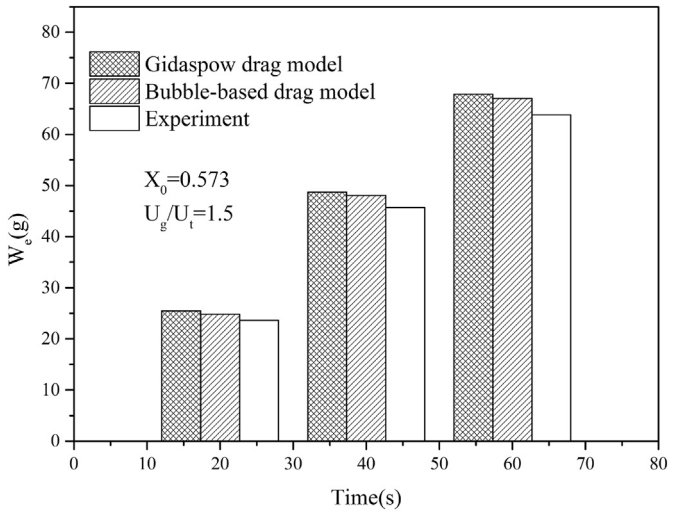

Fig. 2. Comparison of cumulative mass of fines out of the bed between measured data and simulated result.

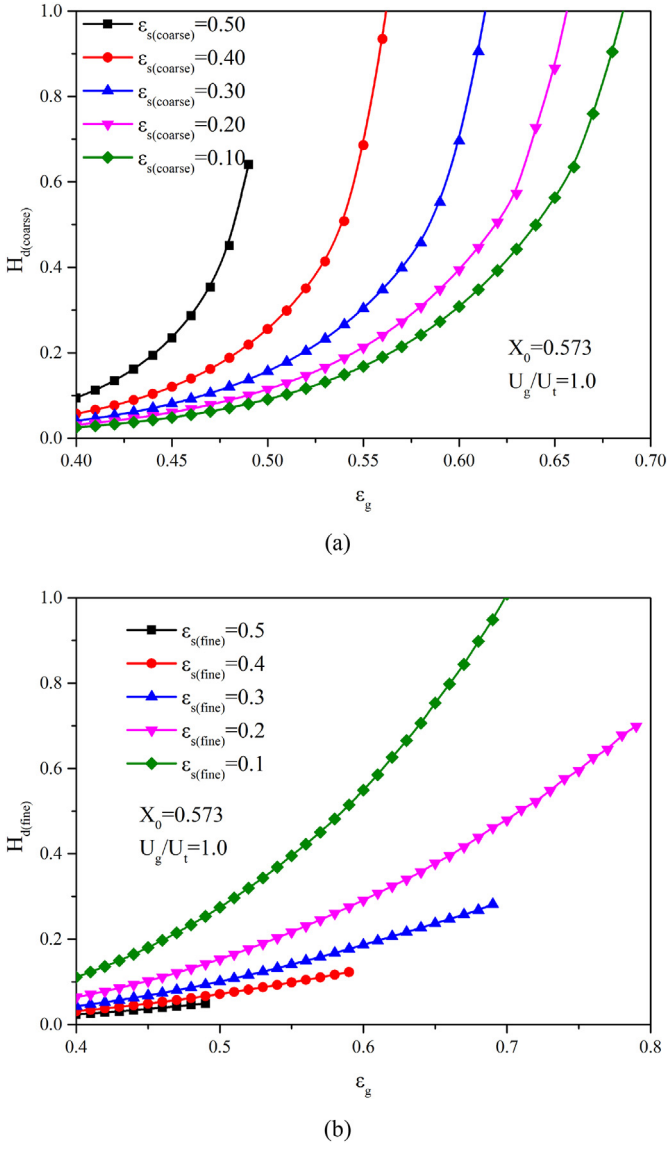

Fig. 3. Variation of heterogeneous index with voidage and solid volume fraction.

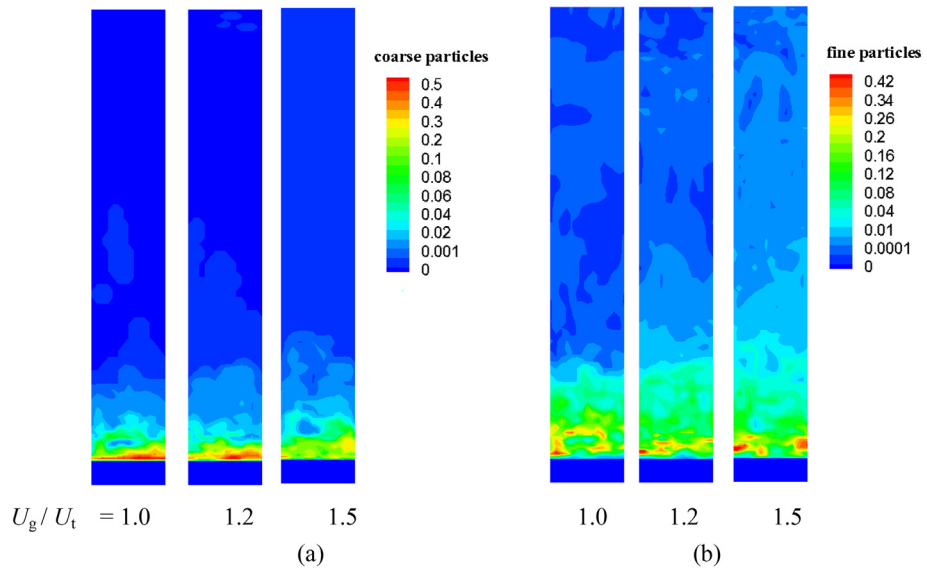

Fig. 4. Contour plots of solid concentrations under different operating velocities ($t = 60$s).

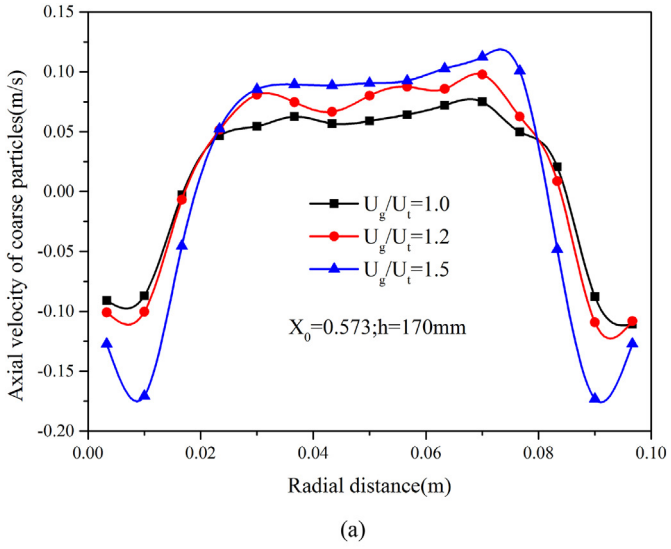

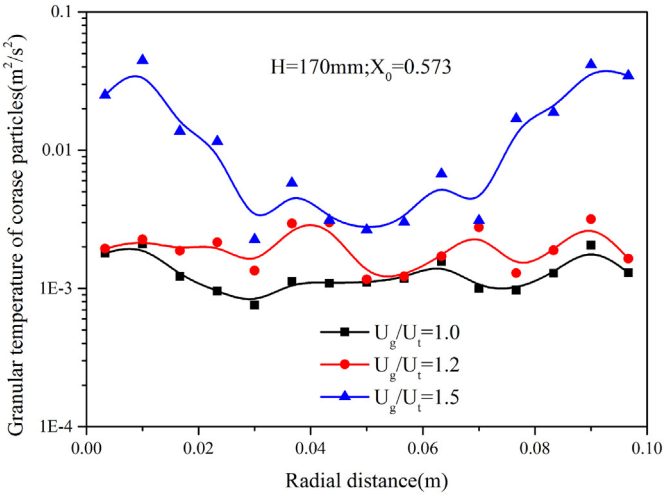

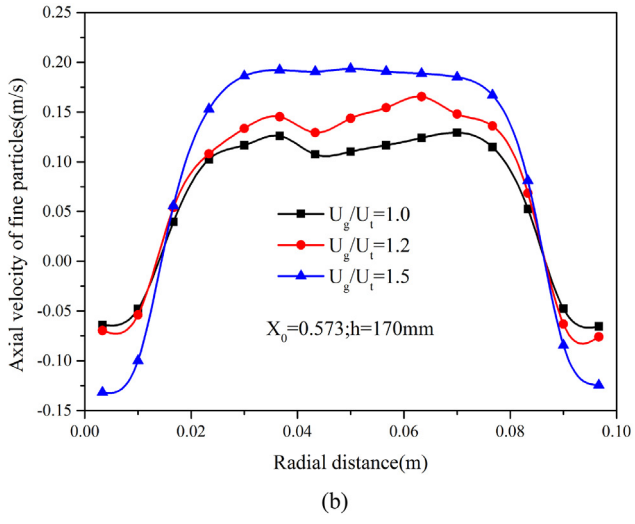

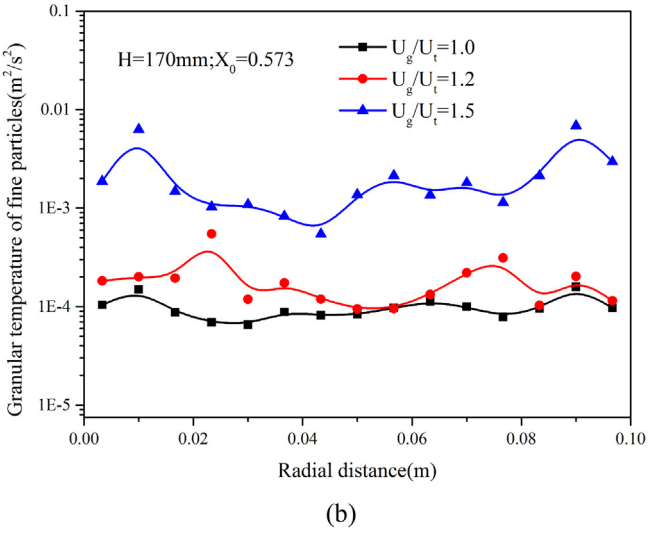

Fig. 5. Lateral profiles of axial solid velocity under different operating velocities.

Fig. 6. Lateral profiles of granular temperature under different operating velocities.

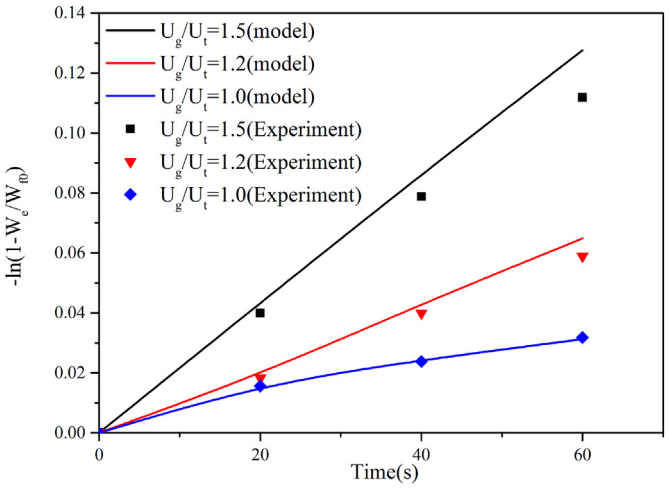

Fig. 7. Relationship between $\ln(1 - W_e/W_{f0})$ and time.

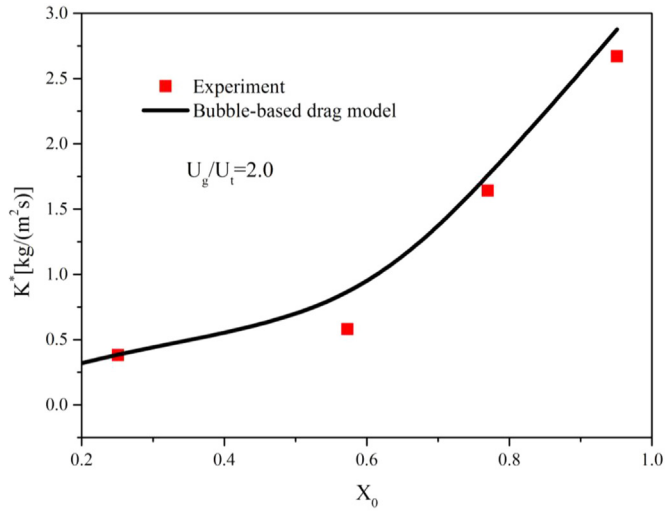

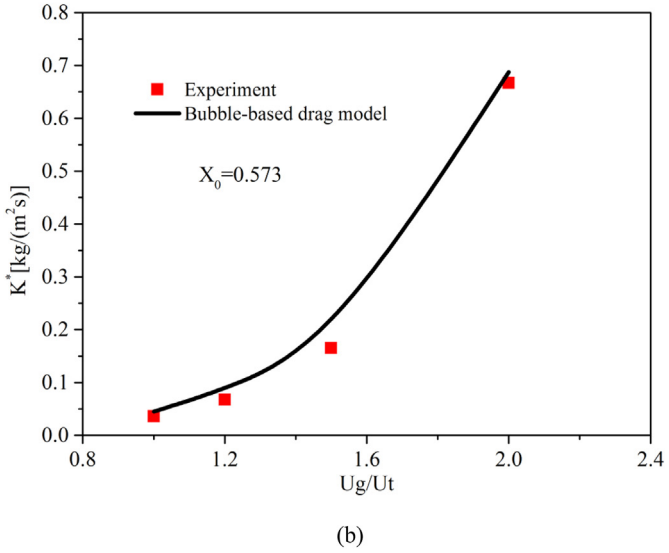

Fig. 8. Effect of operating velocity and initial loading of fines on the elutriation rate constant.

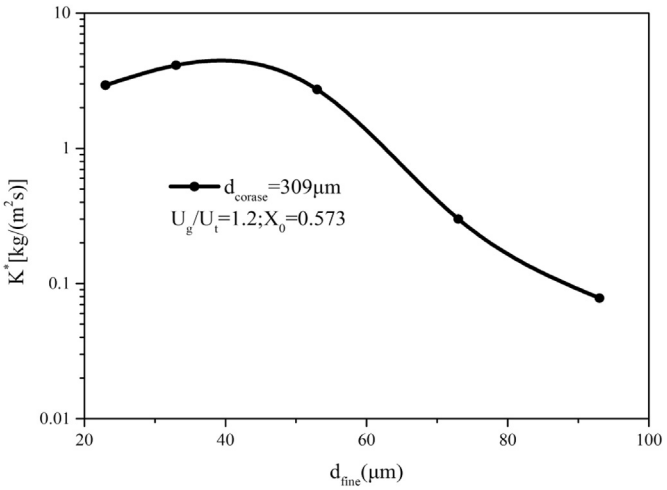

Fig. 9. Effect of fine particle size on the elutriation rate constant.

that the present model can capture the elutriation process of binary mixture.

The particle physical properties determine the elutriation rate. The impact of fine particle size on the elutriation rate constant is evaluated and displayed in Fig. 9. It can be observed that the elutriation rate constant has a clear drop as the fine particle size increases. When the fine particle size is smaller, the increase of particle size will promote the elutriation rate constant. This is attributed to the fact that the adhesion force dominates at a small particle size and the particles tend to form agglomeration or adhere to coarse particles, leading to the reduction of the elutriation rate as the particle size decreases. This phenomenon was also found by the experiments of *Ma* et al. [27].

In the industrial application, some elutriation processes occur under the high-temperature condition. For simplification, the local temperature variation in the bed is neglected. The temperature effect on the heterogeneous index is shown in Fig. 10. We can see that increasing the temperature can reduce the heterogeneous index and the non-uniformity in the bed is enhanced. By comparing the temperature effect on the heterogeneous index of binary mixture, we can find that the heterogeneous index of coarse particles is more sensitive to the temperature, especially for low temperature condition. However, the overall variation of the heterogeneous index of fine particles is not obvious with a small value, which means that the bubble effect on gas-fine particle drag force is more significant.

The effect of operating temperature on the elutriation rate constant is shown in Fig. 11. It can be found that the elutriation rate has an obvious decrease with the increase of the temperature. Here, the variation of gas density with temperature is taken into consideration, neglecting the effect of temperature on particle properties. According to the ideal gas state equation, the increase of bed temperature will reduce the gas density so that the gas driving force becomes weak, resulting in the decrease of fine particle elutriation. This means that the increase of operating temperature is not beneficial to the elutriation process of fine particles.

4. Conclusion

A three-dimensional simulation is carried out to investigate the elutriation process of fines from binary mixture with different aerodynamic characteristics. The multi-fluid model is employed with the bubble-based drag model for the bi-disperse particles system to consider the meso-scale structure effect. The dependence of elutriation rate on operating condition is evaluated. It can be found that at a small particle size, the decrease of particle size reduces the elutriation rate owing to the formation of agglomeration. The simulation results give a good agreement with experimental data. In addition, the impacts

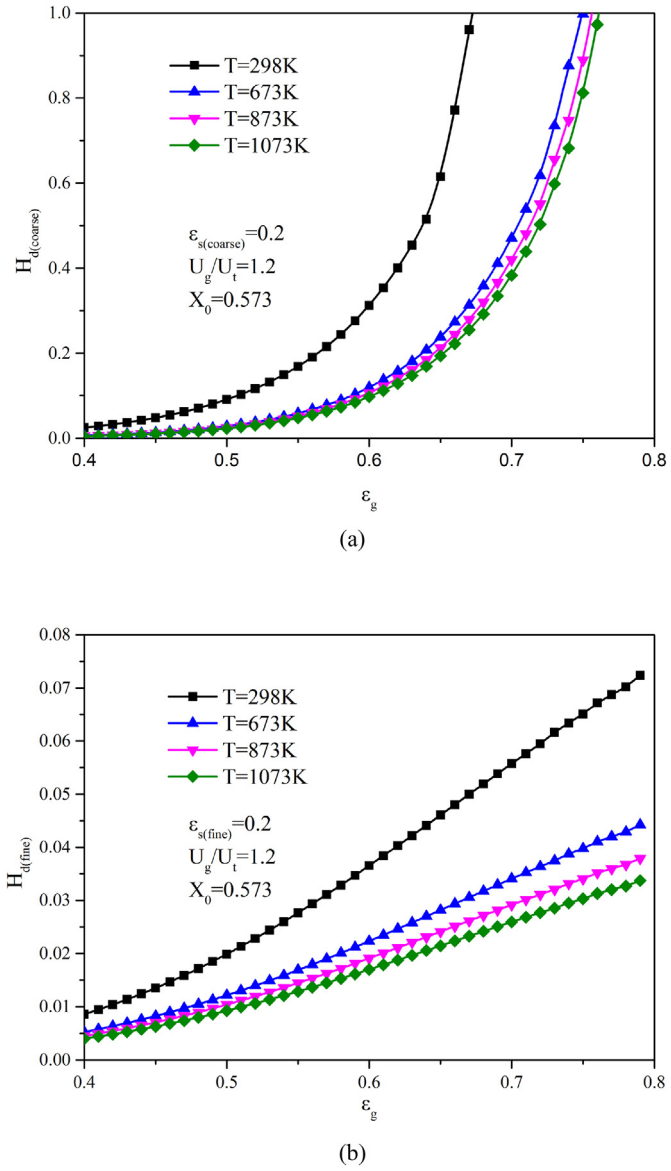

Fig. 10. Variation of heterogeneous index with voidage at different operating temperatures.

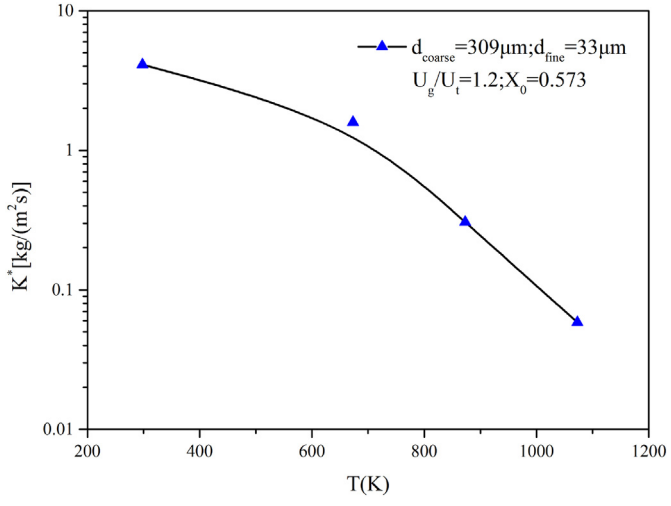

Fig. 11. Effect of operating temperature on the elutriation rate constant.

of bed temperature on the multi-scale drag coefficient and the elutriation rate are further examined. The results reveal that the increase of operating temperature increases the non-uniformity of interphase drag force and weakens the elutriation rate of fine particles.

In the future work, the effect of local temperature variation in the bed will be further taken into account.

Nomenclature

a	acceleration [m s^{-2}]
C_D	drag coefficient of a single particle
d	particle diameter [m]
e	restitution coefficient
F	force acting on each particle or cluster [N]
g_0	radial distribution function
g	gravity [m s^{-2}]
J	collisional energy dissipation [kg m^{-1} s^{-3}]
k	elutriation rate constant [s^{-1}]
K^*	normalized elutriation rate constant [kg m^{-2} s^{-1}]
p	pressure [Pa]
Re	Reynolds number
u	velocity [m s^{-1}]
U	superficial velocity [m s^{-1}]
U_{se}	superficial slip velocity in the emulsion[m s^{-1}]
W_e	cumulative mass of fines out of the bed [g]
W_{f0}	initial total mass in the bed[g]

Greek letters

β	drag coefficient [kg m^{-3} s^{-1}]
ε	volume fraction
θ	granular temperature [m^2 s^{-2}]
μ	viscosity [Pa.s]
ρ	density [kg m^{-3}]
τ	stress tensor [Pa]
δ_b	bubble fraction
$\prod$	kinetic energy production through slip between phase [kg m^{-1} s^{-3}]

Subscripts

b	bubble phase
e	emulsion phase
g	gas phase
p	particle phase
w	wall

Acknowledgments

This research is conducted with financial support from the National Natural Science Foundation of China (51606053), China Postdoctoral Science Foundation funded project (2016T90285) and Chinese Heilongjiang postdoctoral science funding award No. LBH-Z15055.

References

[1] J. Adanez, A. Abad, F. Garcia-Labiano, P. Gayan, L.F. de Diego, Progress in chemical-looping combustion and reforming technologies, Prog. Energ. Combust. 38 (2012) 215–282.
[2] S. Banerjee, R.K. Agarwal, Computational fluid dynamics simulations of a binary particle bed in a riser-based carbon stripper for chemical looping combustion, Powder Technol. 325 (2018) 361–367.
[3] F. Zerobin, S. Penthor, O. Bertsch, T. Pröll, Fluidized bed reactor design study for pressurized chemical looping combustion of natural gas, Powder Technol. 316 (2017) 569–577.

[4] C. Linderholm, A. Lyngfelt, A. Cuadrat, E. Jerndal, Chemical-looping combustion of solid fuels-operation in a 10 kW unit with two fuels, above-bed and in-bed fuel feed and two oxygen carriers, manganese ore and ilmenite, Fuel 102 (2012) 808–822.
[5] L. Chen, J. Bao, L. Kong, M. Combs, H.S. Nikolic, Z. Fan, K. Liu, The direct solid-solid reaction between coal char and iron-based oxygen carrier and its contribution to solid-fueled chemical looping combustion, Appl. Energ. 184 (2016) 9–18.
[6] H. Leion, T. Mattisson, A. Lyngfelt, Solid fuel in chemical looping combustion, Int. J. Greenh. Gas Control 2 (2) (2008) 180–193.
[7] S. Penthor, M. Stollhof, T. Pröll, H. Hofbauer, Detailed fluid dynamic investigations of a novel fuel reactor concept for chemical looping combustion of solid fuels, Powder Technol. 287 (2016) 61–69.
[8] R. Wadhwani, B. Mohanty, Effect of ash on coal direct chemical looping combustion, Int. J. Global Energy 39 (5) (2016) 271–288.
[9] E.R. Monazam, R.W. Breault, J. Weber, K. Layfield, Elutriation of fines from binary particle mixtures in bubbling fluidized bed cold model, Powder Technol. 305 (2017) 340–346.
[10] J.H. Choi, J.M. Suh, I.Y. Chang, D.W. Shun, C.K. Yi, J.E. Son, S.D. Kim, The effect of fine particles on elutriation of coarse particles in a gas fluidized bed, Powder Technol. 121 (2001) 190–194.
[11] M. Azadi, Multi-fluid Eulerian modeling of limestone particles' elutriation from a binary mixture in a gas-solid fluidized bed, J. Ind. Eng. Chem. 17 (2011) 229–236.
[12] S. Schneiderbauer, S. Pirker, Filtered and heterogeneity-based subgrid modifications for gas—solid drag and solid stresses in bubbling fluidized beds, AICHE J. 60 (2014) 839–853.
[13] N. Yang, W. Wang, W. Ge, L.N. Wang, J. Li, Simulation of heterogeneous structure in a circulating fluidized-bed riser by combining the two-fluid model with the EMMS approach, Ind. Eng. Chem. Res. 43 (2004) 5548–5561.
[14] Z. Shi, W. Wang, J. Li, A bubble-based EMMS model for gas-solid bubbling fluidization, Chem. Eng. Sci. 66 (2011) 5541–5555.
[15] W. Wang, J. Li, Simulation of gas-solid two-phase flow by a multi-scale CFD approach-Extension of the EMMS model to the subgrid level, Chem. Eng. Sci. 62 (2007) 208–231.
[16] M. Lungu, Y. Zhou, J. Wang, Y. Yang, A CFD study of a bi-disperse gas-solid fluidized bed: effect of the EMMS sub grid drag correction, Powder Technol. 280 (2015) 154–172.
[17] Q. Zhou, J. Wang, CFD study of mixing and segregation in CFB risers: extension of EMMS drag model to binary gas-solid flow, Chem. Eng. Sci. 122((2015) 637–651.
[18] S. Benyahia, M. Syamlal, T.J. O'Brien, Summary of MFIX Equations 2005–4From URL http://www.mfix.org/documentation/MfixEquations2005-4-3.pdf July 2007.
[19] A. Srivastava, S. Sundaresan, Analysis of a frictional-kinetic model for gas-particle flow, Powder Technol. 129 (2003) 72–85.
[20] S. Wang, K. Zhang, S. Xu, X. Yang, Assessment of a bubble-based bi-disperse drag model for the simulation of a bubbling fluidized bed with a binary mixture, Powder Technol. 338 (2018) 280–288.
[21] D.G. Thomas, Transport characteristics of suspension: VIII. A note on the viscosity of Newtonian suspensions of uniform spherical particles, J. Colloid Interface Sci. 20 (1965) 267–277.
[22] Y.D. Liu, S. Kimura, Fluidization and entrainment of difficult-to-fluidize fine powder mixed with easy-to fluidize large particle, Powder Technol. 75 (1993) 189–196.
[23] M. Leva, Elutriation of fines from fluidized systems, Chem. Eng. Prog. 47 (1951) 39–45.
[24] K. Kato, S. Kanbara, T. Tajima, H. Shibasaki, K. Ozawa, T. Takarada, Effect of particle-size on elutriation rate-constant for a fluidized-bed, J. Chem. Eng. Jpn 20 (1987) 498–504.
[25] J.L. Sinclair, R. Jackson, Gas-particle flow in a vertical pipe with particle-particle interactions, AICHE J. 35 (1989) 1473–1486.
[26] M. Syamlal, MFIX Documentation: Numerical Techniques. DOE/MC-31346-5824. NTIS/DE98002029, National Technical Information Service, Springfield, VA, 1998.
[27] X. Ma, Y. Honda, N. Nakagawa, K. Kato, Elutriation of fine particles from a fluidized bed of a binary particle-mixture, J. Chem. Eng. Jpn. 29 (2) (1996) 330–335.